Cancer Letters 458 (2019) 113–122

Contents lists available at ScienceDirect

Cancer Letters

journal homepage: www.elsevier.com/locate/canlet

Original Articles

Block of NF-kB signaling accelerates MYC-driven hepatocellular carcinogenesis and modifies the tumor phenotype towards combined hepatocellular cholangiocarcinoma

Jiajia He[a,1], Melanie Gerstenlauer[a], Lap Kwan Chan[a], Frank Leithäuser[b], Matthew M. Yeh[c], Thomas Wirth[a,*,3], Harald J. Maier[a,**,2,3]

[a] Institute of Physiological Chemistry, University Hospital of Ulm, Albert-Einstein-Allee 23, 89081, Ulm, Germany
[b] Institute of Pathology, University Hospital of Ulm, Albert-Einstein-Allee 23, 89081, Ulm, Germany
[c] Department of Pathology, University of Washington, 1959 NE Pacific St., Seattle, USA

ARTICLE INFO

Keywords:
Hepatocellular carcinoma (HCC)
Hepatocellular cholangiocarcinoma
MYC
NF-κB
NF-κB essential modulator (NEMO)

ABSTRACT

Primary liver cancer ranks among the leading causes of cancer death worldwide. Risk factors are closely linked to inflammation, such as viral hepatitis and alcoholic as well as non-alcoholic steatohepatitis. Among the pathways involved in the pathogenesis of malignant liver tumors, dysregulation of NF-κB signaling plays a prominent role. It provides a link between inflammation and cancer. To examine the role of NF-κB in a MYC-induced model of hepatocellular carcinoma we deleted NEMO (IKKγ) specifically from hepatocytes. NEMO deletion accelerated tumor development and shortened survival, suggesting a tumor-suppressive function of NF-κB signaling. We observed increased proliferation, inflammation and fibrosis, as well as activation of MAPK and STAT signaling. Importantly, deletion of NEMO modified the tumor phenotype from hepatocellular carcinoma to combined hepatocellular cholangiocarcinoma. The intrahepatic cholangiocarcinoma tumor component showed increased expression of progenitor markers such as Sox9 and reduced expression of mature hepatic markers such as CPS1. In both cases tumorigenesis was reversible by turning off MYC expression.

To our knowledge this is the first mouse model of combined hepatocellular cholangiocarcinoma and may provide insights into the development of this rare malignant tumor.

1. Introduction

Primary liver cancer is the second leading cause of cancer mortality worldwide with an increasing incidence [1]. Risk factors for liver cancer are conditions of continuous liver injury and chronic inflammation, such as infection with HBV and HCV, alcoholic hepatitis, and non-alcoholic steatohepatitis. The NF-κB pathway is a critical modulator of these conditions and represents an important link between inflammation and tumorigenesis [2].

NF-κB is a pleiotropic transcription factor regulating inflammation, innate immunity, cell survival and proliferation. In murine hepatocytes, inhibition of NF-κB activity led directly to the induction of apoptosis [3,4]. The role of NF-κB in liver cancer is contradictory [5]. Some studies showed that NF-κB promotes inflammation-associated cancer [2,6,7], whereas liver-specific NF-κB inactivation can enhance hepatocarcinogenesis and induce spontaneous development of hepatocellular carcinoma (HCC), suggesting that NF-κB may act as tumor suppressor in hepatocytes [8–10]. Another study reported that the NF-κB essential modulator (NEMO), the regulatory kinase subunit upstream of NF-κB, prevents hepatocarcinogenesis by inhibiting hepatocyte apoptosis through NF-κB-dependent and NF-κB-independent functions [11]. These data argue for a context-specific function of NF-κB in liver

Abbreviations: ALP, alkaline phosphatase; ALT, alanine aminotransferase; AST, aspartate aminotransferase; cHCC-CC, combined hepatocellular cholangiocarcinoma; GGT, gamma-glutamyl transferase; HCC, hepatocellular carcinoma; ICC, intrahepatic cholangiocarcinoma; NEMO, NF-κB essential modulator; NF-κB, nuclear factor κB

* Corresponding author.
** Corresponding author.
E-mail addresses: thomas.wirth@uni-ulm.de (T. Wirth), harald.maier@novartis.com (H.J. Maier).
[1] Current address: Oncology Department, The Third Affiliated Hospital of Soochow University, Juqian Street 185, 213003 Changzhou, Jiangsu, China.
[2] Current address: Novartis Oncology, Roonstraße 25, 90429 Nürnberg, Germany.
[3] These authors contributed equally.

https://doi.org/10.1016/j.canlet.2019.05.023
Received 12 March 2019; Received in revised form 16 May 2019; Accepted 19 May 2019

carcinogenesis. The MYC oncogene plays a critical essential role in different cancers, including HCC [12–15].

We combined a mouse model of MYC-induced HCC with liver-specific NEMO deletion. We found that NEMO deletion not only accelerates cancer-progression in MYC-induced carcinogenesis, but also shifts the phenotype from HCC towards combined hepatocellular-cholangiocarcinoma (cHCC-CC), a rare and aggressive subtype of primary liver cancer [16].

2. Materials and methods

2.1. Mice

LAP-tTA mice (expressing the tetracycline transactivator (tTA) under the control of the liver activator protein (LAP) promoter) [17], the tetO-MYC mouse line (bearing a MYC transgene and a luciferase construct under the control of a bidirectional tTA-regulated promoter) [18], the Albumin-Cre mouse line (expressing the Cre recombinase under the control of the albumin promoter) [19] and floxed NEMO mice have been described previously [9,20]. Mice with liver-specific overexpression of MYC ($MYC^{LAP\text{-}tTA}$ mice) were obtained by crossing LAP-tTA mice with tetO-MYC mice. The expression of MYC was conditionally regulated by doxycycline treatment [17]. Mice with liver-specific deletion of NEMO ($NEMO^{\Delta LPC}$) were obtained by crossing Albumin-Cre mice with floxed NEMO mice. Mice with liver-specific overexpression of MYC and liver-specific deletion of NEMO ($NEMO^{\Delta LPC}$) were obtained by crossing together all four genetic modifications and analyzing male mice only. The background of LAP-tTA, Albumin-Cre and mice with a floxed NEMO allele was C57BL/6, and that of tetO-MYC mice was NMRI. All mice used for analysis were on a defined F1 mixed background of C57BL/6 and NMRI. Animal experiments were performed according to German animal welfare laws and approved by the authority (TVA1328).

2.2. In vivo bioluminescence imaging (IVIS)

To indirectly monitor the expression of the MYC transgene, animals of interest were anesthetized with isoflurane and injected with luciferin intraperitoneally. An IVIS Imaging system 200 was used to visualize luciferase activity.

2.3. Measurement of liver serum parameters

Blood samples were centrifuged at 3000 rpm for 10 min at room temperature to collect serum. Serum levels of AST, ALT, ALP, GGT, and bilirubin were measured using a Reflotron system (Roche).

2.4. RNA extraction, cDNA synthesis and quantitative RT-PCR

Livers were snap-frozen in liquid nitrogen and stored at −80 °C. RNA was extracted with RNeasy kit (Qiagen) according to the manufacturer's instructions. 1.5 µg of RNA was used to synthesize cDNA with the Transcriptor High Fidelity cDNA Synthesis Kit (Roche). Quantitative RT-PCR was performed with a Light Cycler 480, using the Universal Probe Library (Roche). Sequences of the used primers are listed in Supplementary Table 1.

2.5. Protein analysis

For protein extraction, liver tissue was pulverized and resuspended in buffer containing 4% SDS, 100 mM Tris-HCl, and protease/phosphatase inhibitors (Roche). Western blotting was carried out according to standard protocols. Membranes were incubated with the primary antibodies listed in Supplementary Table 2. For secondary antibodies, anti-rabbit-HRP, anti-mouse-HRP, and anti-goat-HRP were used.

2.6. Histology and immunostaining

Histology was performed on formalin-fixed and paraffin-embedded liver sections on which hematoxylin-eosin staining was performed. For immunostainings, slides were incubated at 56 °C overnight, fully hydrated with xylene and graded alcohol, placed in distilled water, heated in citrate buffer for 10 min in a pressure cooker, cooled down to room temperature, washed three times in PBS, and blocked with PBS containing 5% BSA for 1 h at room temperature. Slides were incubated with primary antibodies overnight at 4 °C, washed three times in PBS and incubated with secondary antibody for 1 h at room temperature. Nuclear staining was done with DAPI. For immunohistochemistry, the staining was visualized with AEC substrate (DAKO). Antibodies for IHC and IF are listed in Supplementary Tables 3 and 4 Sirius red staining was performed according to the manufacturer's instructions. For quantitative microscopy of Ki67, cleaved caspase 3, α-SMA and Sirius Red, at least six micrographs per section were taken in a blindfolded manner and analyzed with BZ Analyzer software (Keyence). ImageJ was utilized to count Ki67 and cleaved caspase 3 positive cells. Data analysis was done with GraphPad Prism V.6.0. software.

2.7. Statistical analysis

Continuous variables are presented as mean ± SD. Student's t-test was used to compare groups of independent samples to corresponding group. Two-way ANOVA was used to compare the effect of two different categorical independent variables on one continuous dependent variable. p values of $p < 0.05$ were considered statistically significant (*$p < 0.05$, **$p < 0.01$, ***$p < 0.001$, ****$p < 0.0001$, ns, not significant).

3. Results

For liver-specific MYC expression we used a model similar to previously described hepatocellular carcinoma models driven by MYC [12,15,21], however using a different MYC founder line [18]. In these mice, MYC expression is regulated by the hepatocyte-specific expression of the tetracycline-regulated transactivator provided by the LAP-tTA mouse line (Fig. 1A). To avoid any effect of MYC expression during liver development, mice were treated with doxycycline until birth and MYC expression was activated by doxycycline removal after birth. Since the expression of the MYC transgene is coupled to a luciferase reporter, we were able to monitor transgene expression by in vivo chemoluminescence. Strong expression of luciferase was detectable in $MYC^{LAP\text{-}tTA}$ mice 6 weeks after doxycycline removal (Fig. 1B). For deletion of NEMO, we used the well-established albumin-Cre mouse line and combined it with mice bearing a floxed allele of NEMO [20]. The combination of all these genetically modified mouse lines resulted in mice that expressed MYC in a liver-specific fashion ($MYC^{LAP\text{-}tTA}$) and had deleted NEMO in hepatocytes ($NEMO^{\Delta LPC}$).

Expression of MYC and deletion of NEMO was verified by immunoblotting (Fig. 1C). Expression of MYC was not affected by NEMO deletion. There was a background NEMO signal in $NEMO^{\Delta LPC}$ mice, which may be explained by the fact that NEMO was only deleted in the parenchymal cells of the liver. The slight signal increase in livers of $MYC^{LAP\text{-}tTA}/NEMO^{\Delta LPC}$ mice was most likely due to increasing numbers of infiltrating cells, in which NEMO was not deleted. In addition to immunoblotting, over-expression of MYC protein was also verified by immunofluorescence on liver sections from mice bearing the MYC transgene in the presence or absence of NEMO (Fig. 1D).

We first studied tumor development in our mouse model of MYC-induced liver carcinogenesis without interfering with NEMO: Indeed almost all $MYC^{LAP\text{-}tTA}$ mice developed liver tumors. Detailed analyses revealed that 50% of the animals had reached endpoint disease (as defined in accordance with animal welfare laws and guidelines) by the age of 87 days, whereas in few cases the endpoint was reached at later

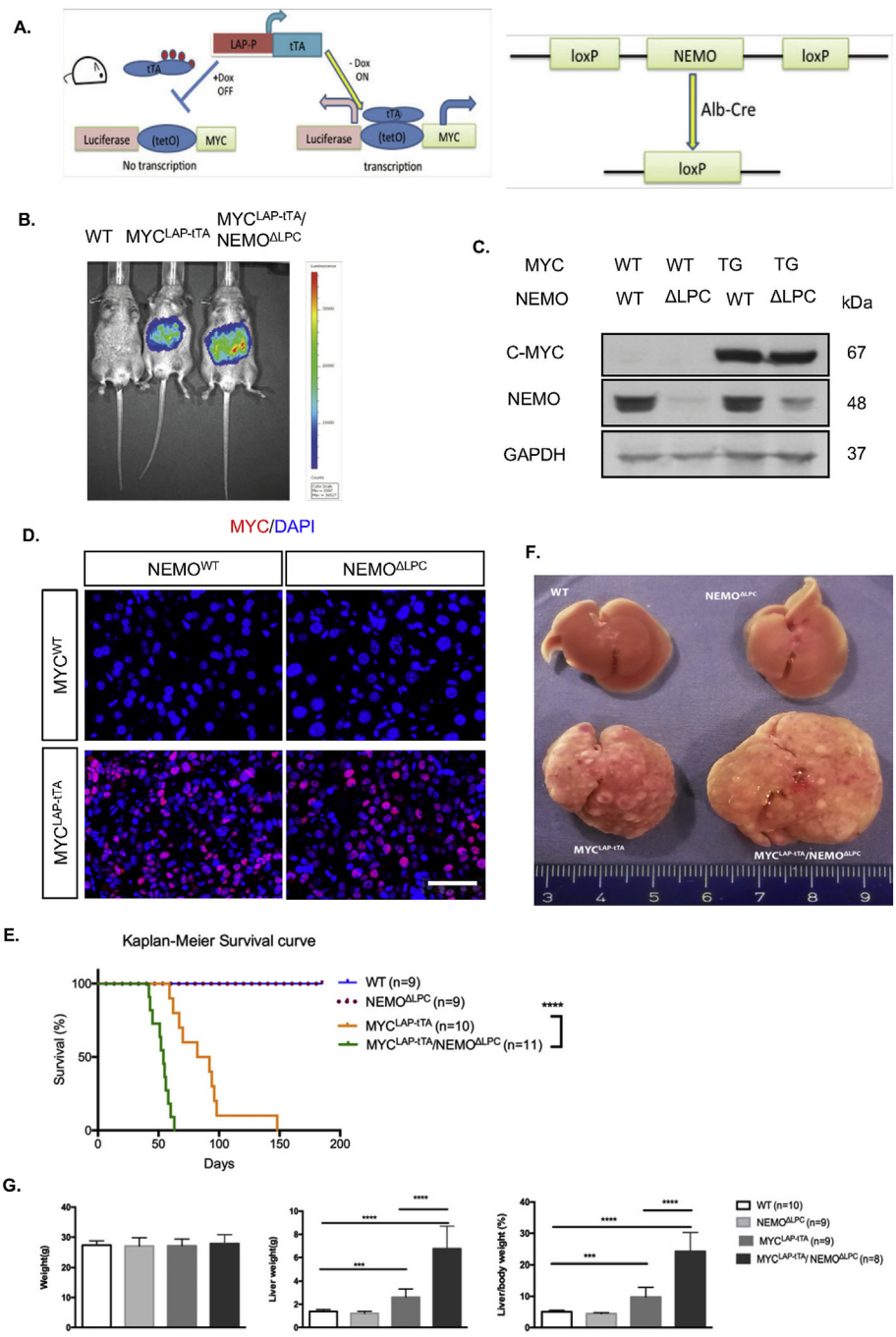

Fig. 1. Liver-specific NEMO deletion alters the survival and phenotype of a mouse model of MYC-induced hepatocellular carcinoma. (A) Left: A Tet-Off system was used to generate transgenic mice that specifically overexpress MYC in the liver. LAP-tTA mice express the tetracycline transactivator (tTA) protein under the control of the liver activator protein (LAP) promoter (LAP-P). The transgene MYC can be repressed conditionally by administration of doxycycline (Dox) in the drinking water of mice and activated by removal of doxycycline. Right: Alb-Cre transgenic mice, expressing Cre recombinase driven by the albumin promoter, were crossed with mice with a *lox*P-flanked ("floxed") NEMO allele in order to delete NEMO from hepatocytes. (B) Representative in vivo bioluminescence imaging showing strong luminescence in projection to the liver area of mice with MYC overexpression. (C) Western blotting of whole liver extracts from mice at the age of 45 days with the respective genotype (WT, wild type for MYC; TG, transgenic for liver-specific MYC expression; ΔLPC, liver parenchymal cell-specific ablation of NEMO) showing liver-specific modulation of MYC and NEMO. GAPDH shown as a loading control. (D) Immunofluorescence staining showing abundant MYC-positive cells in mice with MYC overexpression. Scale bar: 50 μm. (E) Survival (as defined by humane endpoints in accordance with animal welfare regulations) of $MYC^{LAP\text{-}tTA}/NEMO^{\Delta LPC}$ mice (green graph, n = 11 mice) in comparison to $MYC^{LAP\text{-}tTA}$ mice (orange graph, n = 10 mice); ****p < 0.0001 by Log-rank (Mantel-Cox) test. $NEMO^{\Delta LPC}$ (purple graph, n = 9 mice) and wild type mice (WT, blue graph, n = 9 mice) shown as control. (F) Representative macroscopic view of livers from mice with the indicated genotypes at the age of 45 days. (G) Body weight, liver weight and liver weight to body weight ratio of mice with the indicated genotypes at the age of endpoint disease. Shown is the mean ± SD. *p < 0.05, **p < 0.01, ***p < 0.001, ****p < 0.0001, ns, not significant (Mann Whitney test).

time points (up to 148 days) (Fig. 1F, orange graph). This time course is similar to other reports on mice with activation of MYC transgene expression in neonatal hepatocytes [15]. Macroscopic analyses of the livers of these mice revealed substantially enlarged livers with multiple macroscopically visible tumor nodules (Fig. 1F, lower left liver). Microscopically, these nodules showed features of hepatocellular carcinoma, including thickened trabeculi of the hepatocytic cords, pseudoacinar formation, and absence of normal structures (i.e., portal tracts). Steatosis was detectable within some carcinoma cells, a common finding in hepatocellular carcinoma. Carcinoma cells also demonstrated evidence of malignancy like increased nuclear-cytoplasmic ratio, hyperchromatic nuclei, prominent nucleoli and mitotic figures.

When $NEMO^{\Delta LPC}$ mice (without MYC overexpression) were analyzed, not a single mouse developed overt signs of disease (Fig. 1E, purple graph). However, when MYC overexpression was combined with NEMO deletion, our analysis revealed that disease progression was substantially accelerated, with 50% of mice reaching endpoint disease at the age of 54 days already (Fig. 1E, green graph). Livers of these mice macroscopically appeared enlarged compared to the livers of $MYC^{LAP\text{-}tTA}$ mice and also showed a large number of individual tumor nodules (Fig. 1F). As some of the $MYC^{LAP\text{-}tTA}/NEMO^{\Delta LPC}$ mice reached endpoint disease at the age of 45 days, we used this time point for most of the subsequent analyses. At this time point, both the $MYC^{LAP\text{-}tTA}$ mice and the $MYC^{LAP\text{-}tTA}/NEMO^{\Delta LPC}$ mice showed an increase in liver weight and an increase in the liver weight to body weight ratio (Fig. 1G). Development of liver pathology was analyzed using serum markers, such as transaminases ALT and AST, GGT, ALP and bilirubin (Fig. 2A). Serum AST and ALT, and to some degree also ALP and bilirubin (but not GGT), were increased upon NEMO deletion alone at the age of 45 days. In

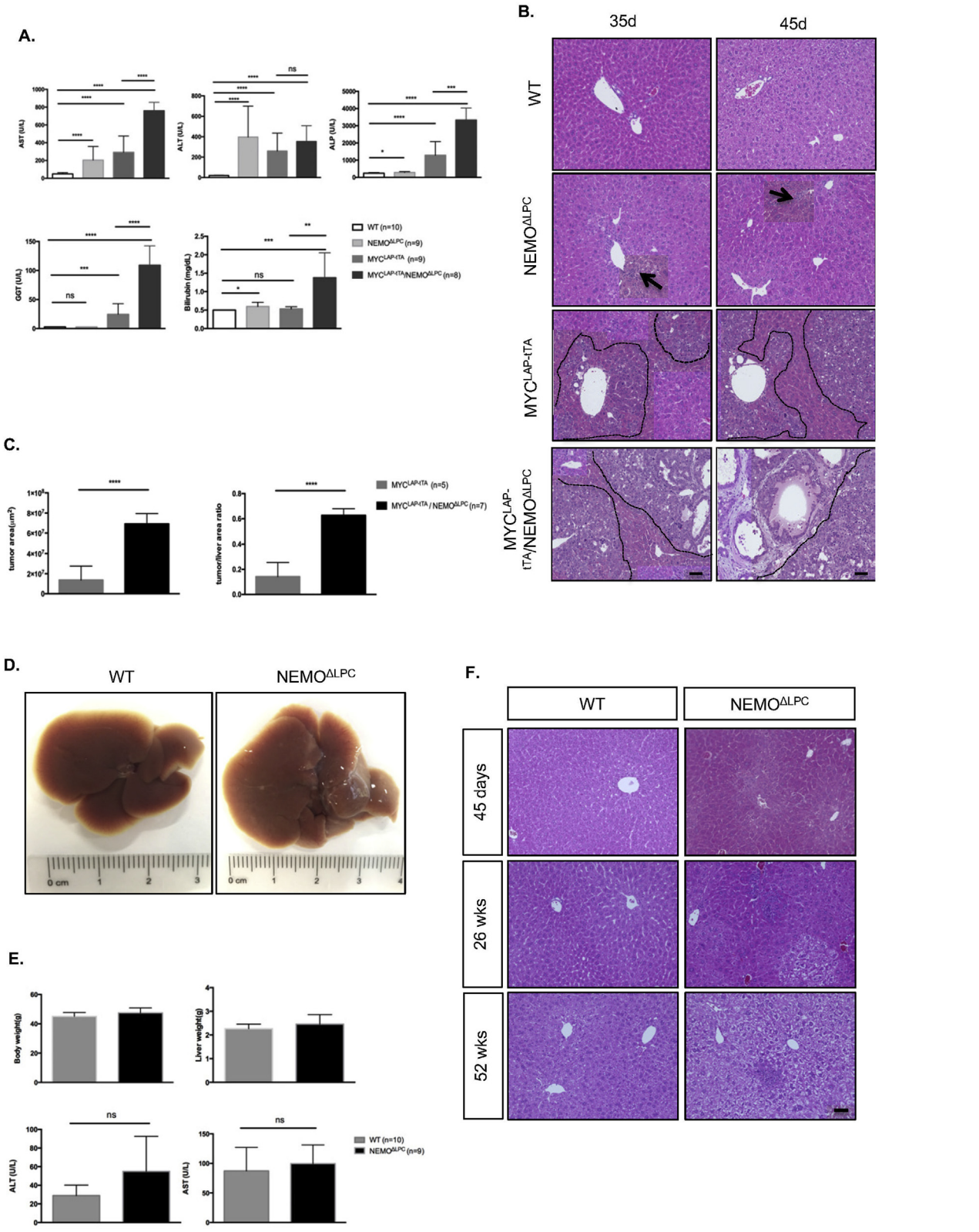

(caption on next page)

MYC$^{LAP\text{-}tTA}$ mice, AST and ALT as well as ALP, GGT and bilirubin levels were significantly elevated but even further increased in MYC$^{LAP\text{-}tTA}$/NEMO$^{\Delta LPC}$ mice (Fig. 2A).

At the age of 45 days no tumors could be seen in either wild type or NEMO$^{\Delta LPC}$ mice by histological analysis. In contrast, MYC$^{LAP\text{-}tTA}$ livers showed multiple tumor nodules of atypical hepatocytes with a predominantly solid or trabecular growth pattern characteristic of HCC (Fig. 2B). Interestingly, the histology of MYC$^{LAP\text{-}tTA}$/NEMO$^{\Delta LPC}$ livers was strikingly different. Unlike the tumors in the MYC$^{LAP\text{-}tTA}$ mice, which only presented as cohesive and solid tumor nodules with thickened trabecular structures, many tumor nodules in the MYC$^{LAP\text{-}tTA}$/NEMO$^{\Delta LPC}$ mice contained not only the HCC component, which still

Fig. 2. NEMO deletion modifies MYC-induced tumorigenesis. (A) Serum levels of AST, ALT, ALP, GGT and bilirubin in mice with the indicated genotype at the time of endpoint disease. Shown is the mean ± SD. *p < 0.05, **p < 0.01, ***p < 0.001, ****p < 0.0001, ns, not significant (Mann Whitney test) (B) H&E staining of representative hepatic tissue sections of mice with the indicated genotypes at the age of 35 days and 45 days. Scale bars: 50 μm. The arrows show areas without evidence of neoplasm, i.e., the presence of portal tracts in $NEMO^{\Delta LPC}$ mice. $MYC^{LAP\text{-}tTA}$ mice developed hepatocellular carcinoma that show thickened trabeculi, pseudoacini, and paucity of portal tracts. The carcinoma cells also demonstrate increased nucleus to cytoplasmic ratio, hyperchromatic nuclei, prominent nucleoli and mitotic figures. $MYC^{LAP\text{-}tTA}/NEMO^{\Delta LPC}$ tumors not only showed a hepatocellular carcinoma component (top), but also a component of cholangiocarcinoma (bottom), characterized by carcinomatous glands lined by cuboidal epithelium (morphologically with biliary differentiation) and surrounded by desmoplastic stroma. These two components intermix intimately at the interface. (C) Quantification of tumor area and tumor area to liver area ratio on sections from mice with the indicated genotype at the age of 35 days (****p < 0.0001, *t*-test). (D) Representative macroscopic view of livers from 52 weeks old wild type (WT) and $NEMO^{\Delta LPC}$ mice. (E) Body weight, liver weight, serum ALT and AST levels of 52 week-old wild type and $NEMO^{\Delta LPC}$ mice. (F) H&E staining of wild type and $NEMO^{\Delta LPC}$ mice at the indicated time points. Scale bar: 50 μm.

showed steatosis in the carcinoma cells, but also a component of cholangiocarcinoma. The cholangiocarcinoma component was characterized by multiple carcinomatous glands lined by cuboidal epithelium, morphologically recapitulating biliary differentiation and surrounded by desmoplastic stroma. These two components intermixed with each other intimately at the interface, reminiscent of combined hepatocellular cholangiocarcinoma in human pathology (Fig. 2B). The total area of liver tumors was substantially enlarged in the $MYC^{LAP\text{-}tTA}/NEMO^{\Delta LPC}$ mice (Fig. 2C).

In order to understand the development of these tumors, we analyzed livers from mice at a younger age. At the age of 5 weeks (35 days), we already saw a striking difference between the $MYC^{LAP\text{-}tTA}$ and the $MYC^{LAP\text{-}tTA}/NEMO^{\Delta LPC}$ mice, with the latter already developing multiple additional cysts/glandular structures within the tumor mass (Fig. 2B). Similar structures have been described in human intrahepatic cholangiocarcinoma (ICC), a primary liver tumor arising from cholangiocytes and clearly distinct from HCC [22]. The total tumor area at this early time point was already markedly increased in $MYC^{LAP\text{-}tTA}/NEMO^{\Delta LPC}$ mice compared to $MYC^{LAP\text{-}tTA}$ mice (Fig. 2C).

$NEMO^{\Delta LPC}$ mice were also analyzed at the age of 26 and 52 weeks, and found no macroscopic signs of HCC or steatohepatitis were detected, despite signs of liver damage were present even at younger ages (Fig. 2D–F). This contrasts to another report of NEMO ablation in hepatocytes, which led to steatohepatitis and HCC, were a different Cre-line was used, however [9].

The larger tumor mass in $MYC^{LAP\text{-}tTA}/NEMO^{\Delta LPC}$ mice could be a consequence of enhanced proliferation. We measured proliferation Ki67 staining and saw a strong increase in the MYC-driven tumors, as expected (Fig. 3A). Also consistent with previous work, there was some increase in proliferation in mice with hepatocyte-specific NEMO deletion. However, the highest level of proliferation was detected in $MYC^{LAP\text{-}tTA}/NEMO^{\Delta LPC}$ mice (Fig. 3A).

Both MYC and NEMO/NF-κB may also affect levels of apoptosis, which we analyzed by staining for cleaved caspase 3. There was a slight increase in apoptosis in MYC-induced tumors as well as NEMO-deficient livers; the most striking increase, however, was seen in $MYC^{LAP\text{-}tTA}/NEMO^{\Delta LPC}$ mice (Fig. 3A). The expression level of proliferation and apoptosis was further verified by quantification of Ki67 staining and cleaved caspase 3 staining (Fig. 3B). The increased apoptotic signals corresponded to the increased apoptotic bodies seen microscopically in these tumors. Inflammation plays an important role in hepatocarcinogenesis and is also linked to NEMO/NF-κB. CD45-positive inflammatory cells were increased moderately in both MYC-transgenic mice and in mice with hepatocyte-specific NEMO ablation; however, the highest levels of infiltration and inflammation were detected in the $MYC^{LAP\text{-}tTA}/NEMO^{\Delta LPC}$ mice (Fig. 3A, Supplementary Fig. 1). Similarly, in regard to fibrosis, there was a slight increase in livers from the $MYC^{LAP\text{-}tTA}$ and the $NEMO^{\Delta LPC}$ mice, whereas highest levels of fibrosis were seen in the $MYC^{LAP\text{-}tTA}/NEMO^{\Delta LPC}$ mice (Fig. 3A).

Next, we analyzed signaling pathways that might be involved in the accelerated and enhanced tumorigenesis in $MYC^{LAP\text{-}tTA}/NEMO^{\Delta LPC}$ mice. IL-6/STAT3 signaling, the RAF/MEK/ERK as well as the p38 and JNK pathways were all induced in the liver tumors, consistent with previous reports [23,24]. RAF/MEK/ERK as well as STAT3 signaling again appeared stronger in the $MYC^{LAP\text{-}tTA}/NEMO^{\Delta LPC}$ mice, compared to MYC-overexpressing mice in the presence of NEMO (Fig. 3C–E).

Since the cystic/glandular tumor component in $MYC^{LAP\text{-}tTA}/NEMO^{\Delta LPC}$ mice resembled intrahepatic cholangiocarcinoma, further immunohistochemical analyses were performed to characterize the precise phenotype. Whereas normal hepatocytes as well as the HCC cells in the MYC-induced tumors stained positive for the hepatocyte-specific marker carbamoyl phosphate synthetase 1 (CPS1), the tumors in the $MYC^{LAP\text{-}tTA}/NEMO^{\Delta LPC}$ mice were largely negative for this hepatocyte-specific marker in their HCC component. In contrast, many cells of the cholangiocarcinoma component in the $MYC^{LAP\text{-}tTA}/NEMO^{\Delta LPC}$ tumors stained positive for cytokeratin 19 (CK19) as well as the transcription factor Sox9, whereas the HCC component in $MYC^{LAP\text{-}tTA}/NEMO^{\Delta LPC}$ tumors was negative for CK19 (Fig. 4A). It had been reported that hepatic stellate cells expressing α-smooth muscle actin (α-SMA) promote hepatocellular carcinoma cell and biliary cell proliferation and correlate with poor prognosis in HCC and cholangiocarcinoma [25–27] and may serve as a source of liver progenitor cells [28]. Indeed, we could observe a significant increase of α-SMA-positive cells in the $MYC^{LAP\text{-}tTA}/NEMO^{\Delta LPC}$ mice in immunofluorescence analyses (Fig. 4B). We confirmed these findings by immunoblotting, which again showed the strongest expression of CK19, Sox 9 and α-SMA in $MYC^{LAP\text{-}tTA}/NEMO^{\Delta LPC}$ livers (Fig. 4C). Except for *Afp*, expression levels of other hepatic progenitor markers like *Krt19*, *Krt7* and *Epcam* was increased in $MYC^{LAP\text{-}tTA}/NEMO^{\Delta LPC}$ livers compared to $MYC^{LAP\text{-}tTA}$ mice (Fig. 4D).

MYC inactivation was shown to result in a rapid and sustained tumor regression in a comparable conditional MYC-HCC mouse model [12]. We thus asked whether the tumors in $MYC^{LAP\text{-}tTA}/NEMO^{\Delta LPC}$ mice would also regress upon MYC inactivation. Doxycycline treatment was therefore resumed in $MYC^{LAP\text{-}tTA}$ and $MYC^{LAP\text{-}tTA}/NEMO^{\Delta LPC}$ mice from the age of 40 days when tumors in these mouse lines are established. Mice were analyzed either 10 days or 4 weeks after shutting off transgenic MYC expression. No luciferase activity was detectable by in vivo immunofluorescence imaging three days after doxycycline re-administration, confirming repression of transgene expression (Fig. 5A). The increased liver weight and liver weight to body weight ratio both in $MYC^{LAP\text{-}tTA}$ and $MYC^{LAP\text{-}tTA}/NEMO^{\Delta LPC}$ animals at 40 days was normalized after 4 weeks of doxycycline treatment (Fig. 5B). Similarly, the increase of AST, ALT and ALP levels at 40 days was a significantly reduced after 4 weeks doxycycline treatment (Fig. 5B). Macroscopically, the livers seemed to be normal after 10 days and 4 weeks of treatment with doxycycline, in both $MYC^{LAP\text{-}tTA}$ and $MYC^{LAP\text{-}tTA}/NEMO^{\Delta LPC}$ animals (Supplementary Fig. 2). Histologically, livers of $MYC^{LAP\text{-}tTA}$ animals appeared normal as well after 10 days treatment, but interestingly, this was not the case in $MYC^{LAP\text{-}tTA}/NEMO^{\Delta LPC}$ animals (Fig. 5C). Although we could not detect tumor nodules after doxycycline treatment in $MYC^{LAP\text{-}tTA}/NEMO^{\Delta LPC}$ animals, there were still abnormal biliary ducts and inflammatory infiltrates in the periportal area (Fig. 5C). Furthermore, these residual structures were still largely negative for the hepatocyte differentiation marker CPS1 (Supplementary Fig. 3) and positive for the progenitor/biliary duct marker CK19 (Fig. 5D), indicating that these cells were still biliary cells or had not transformed back to normal hepatocytes. We also determined the proliferation and

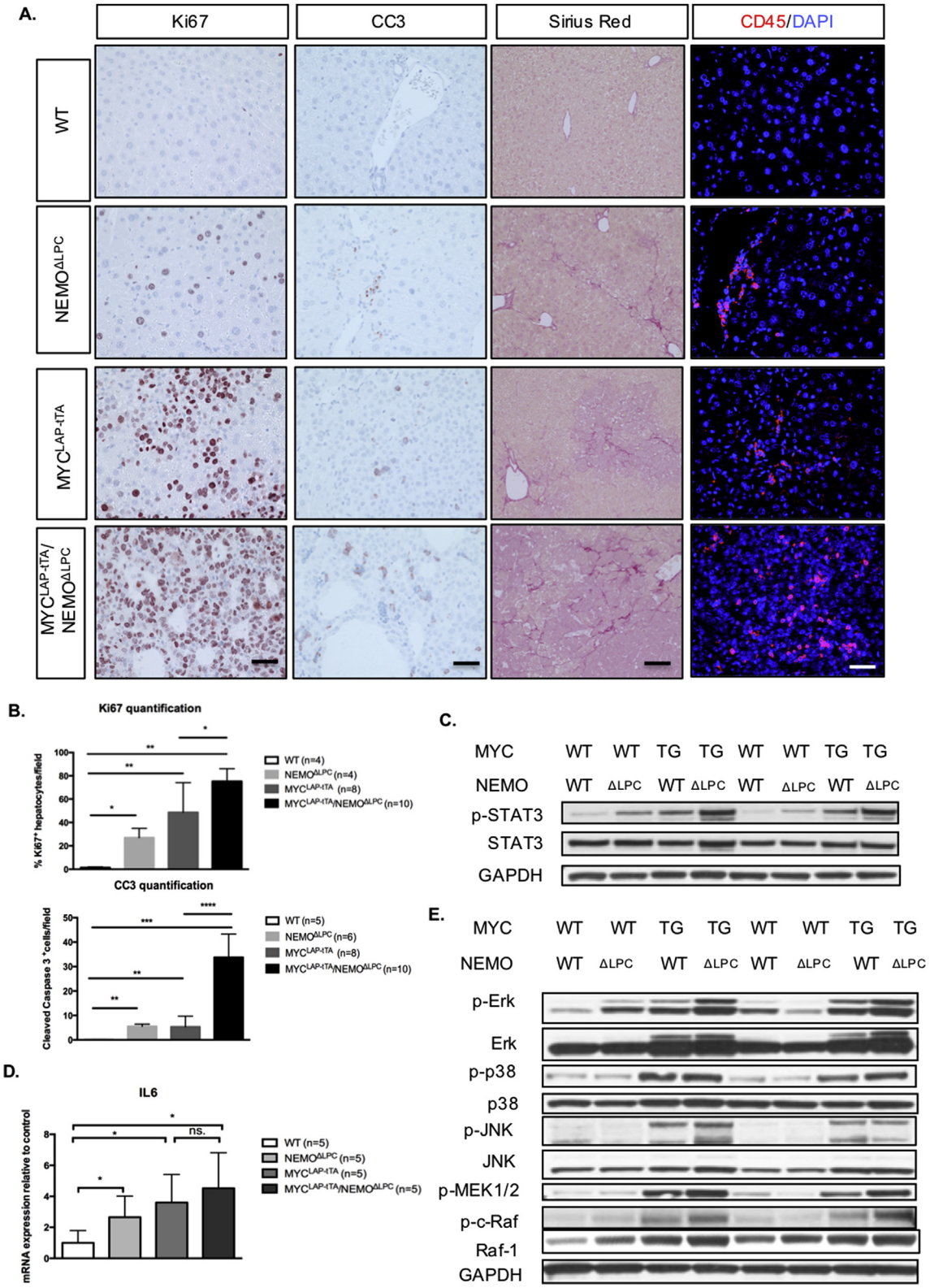

Fig. 3. NEMO deletion increases proliferation, apoptosis, fibrosis and inflammation in MYC-driven HCC mice. (A) Immunohistochemical stainings of Ki67 and cleaved caspase 3 (CC3) as well as sirius red staining for collagen and immunofluorescence staining of CD45 are shown on sections of livers of animals at the age of 35 days. Scale bars: 50 μm. (B) Quantification of immunohistochemical stainings for Ki67 and CC3 positive cells (N ≥ 4 mice/group). (C) Western blotting of liver extracts from mice with the indicated genotypes (WT, wild type for MYC; TG, transgenic for liver-specific MYC expression; ΔLPC, liver parenchymal cell-specific ablation of NEMO) for p-STAT3 and STAT3; GAPDH shown as loading control. (D) Quantitative RT-PCR for IL-6 transcripts in liver tissue of mice at the age of 45 days. Results are shown relative to wild mice, which were set to 1. (E) Western blotting of liver extracts from mice with the indicated genotypes at the age of 45 days for MAPK signaling components. GAPDH was used as a loading control.

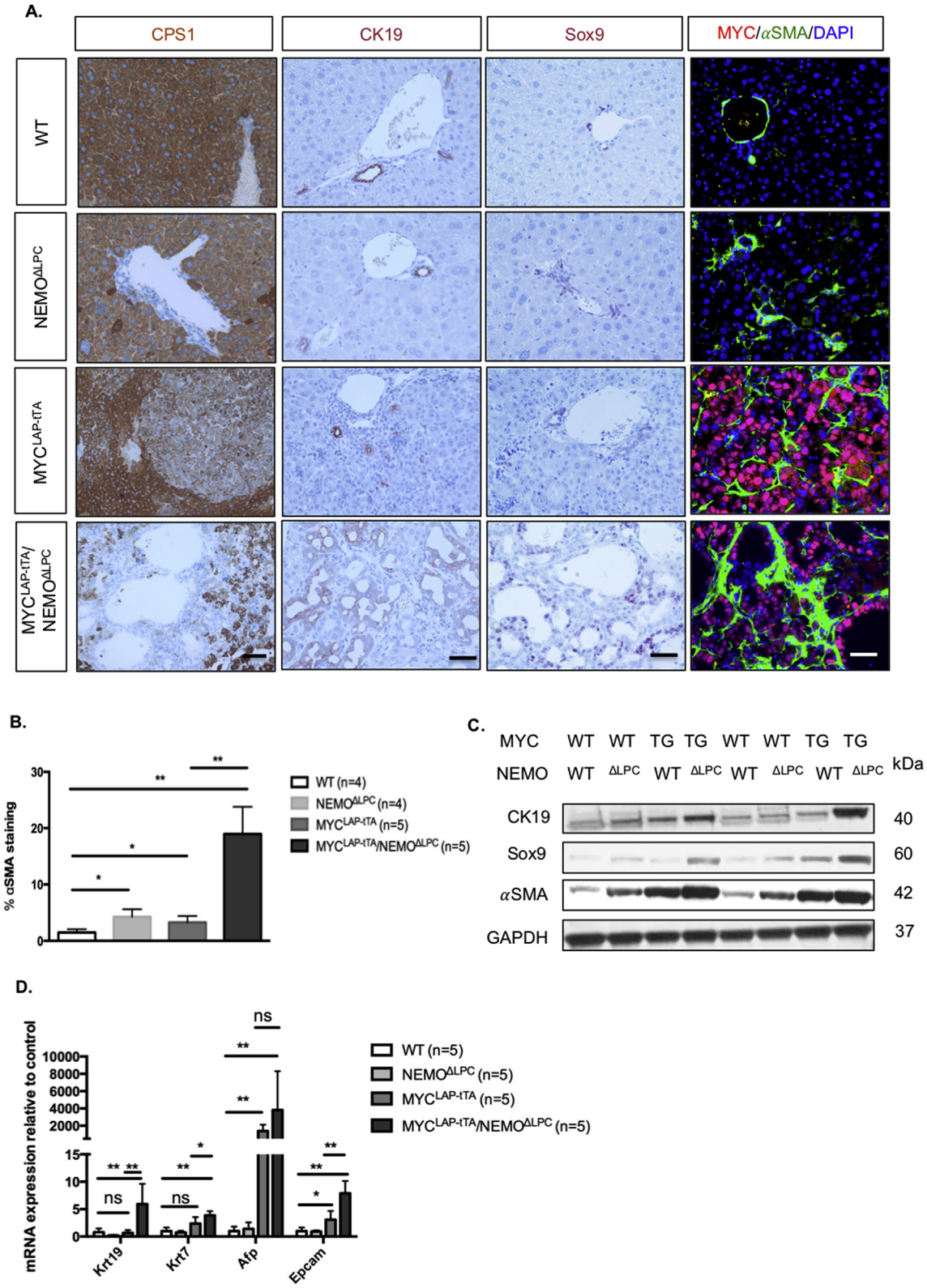

Fig. 4. Tumors developing in MYC$^{LAP\text{-}tTA}$/NEMO$^{\Delta LPC}$ mice possess features of liver progenitor cells. (A) Immunohistochemical staining of CPS1, CK19, Sox9, and immunofluorescence co-staining for α-SMA (green) and MYC (red) on liver sections, DAPI (blue) for nuclear staining. Scale bars: 50 μm. (B) Quantification of α-SMA-positive cells on liver sections of mice at the age of 45 days. (*p < 0.05, **p < 0.01, Mann-Whitney test). (C) Western blotting with antibodies against CK19, Sox9 and α-SMA on liver extracts from mice at the age of 45 days. GAPDH was used as a loading control. (D) Quantitative RT-PCR for Krt19, Krt7, Afp and Epcam transcripts from liver extracts of mice at the age of 45 days with the indicated genotypes. Values are given relative to wild type mice, which were set to 1. N = 5 mice. *p < 0.05, **p < 0.01, ns, not significant (Mann Whitney test).

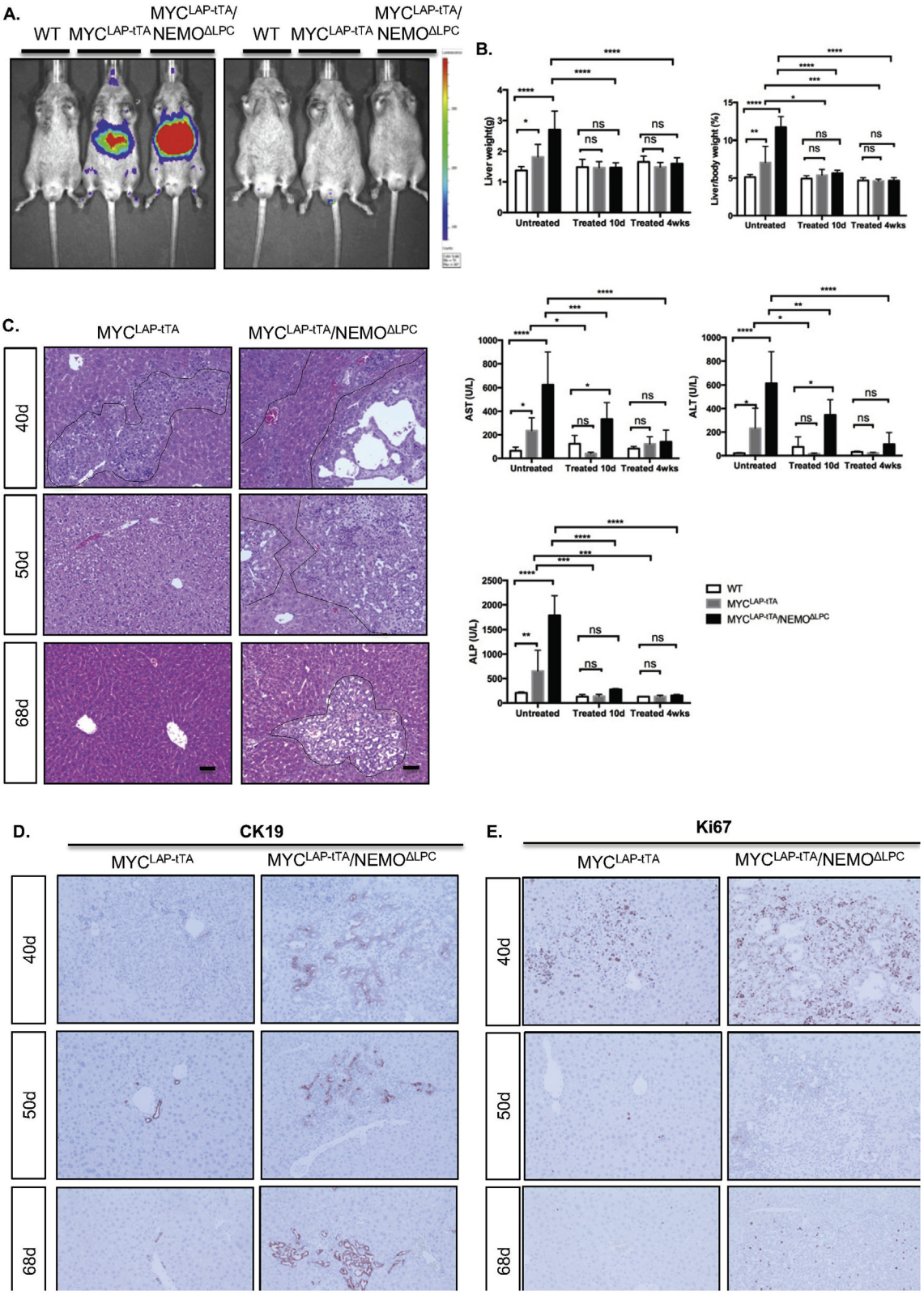

Fig. 5. MYC-induced tumor formation is reversible after switching off MYC transgene expression by administration of doxycycline. (A) Representative in vivo bioluminescence imaging showed strong luminescence activity before doxycycline treatment at 40 days of age (left) and almost no luminescence signal three days after doxycycline treatment (right). (B) Liver weight, liver weight to body weight ratio, serum levels of AST, ALT and ALP of animals before doxycycline re-administration (age: 40 days) and 10 days (age: 50 days) and 4 weeks (age: 68 days) after doxycycline re-administration. N ≥ 5 mice/group. *p < 0.05, **p < 0.01, ***p < 0.001, ****p < 0.0001, ns, not significant (two-way ANOVA test). (C) H&E staining of mice before and after doxycycline treatment (as described in B), showing the disappearance of HCC and ICC components after treatment. Ductular reaction appeared after treatment, which differed significantly from the malignant glands in ICC. (D) Immunohistochemical staining of CK19 before and after doxycycline treatment. (E) Immunohistochemical staining of Ki67 before and after doxycycline treatment (as described in B). Scale bars: 50 μm.

apoptosis levels in $MYC^{LAP\text{-}tTA}$ and $MYC^{LAP\text{-}tTA}/NEMO^{\Delta LPC}$ animals after doxycycline treatment, which showed that MYC inactivation led to a substantially reduced proliferative ability in both groups (Fig. 5E), as well as less apoptosis (Supplementary Fig. 4).

4. Discussion

We developed a mouse model of MYC-induced HCC that recapitulates important steps of HCC development and which is similar to previously published MYC-driven mouse models of primary liver cancer. Here we used this mouse model to elucidate the role of NEMO in MYC-induced primary liver cancer by combining liver-specific MYC overexpression with liver-specific deletion of NEMO.

Our study provides evidence for the importance of NF-κB as a tumor suppressor, since the growth of MYC-induced primary liver tumors was significantly accelerated by the loss of NEMO. Liver-specific deletion of NEMO using the ALFP-Cre mouse line resulted in development of steatohepatitis and HCC [9]. Although there was some degree of damage as evidenced by serum markers and liver histology, our $NEMO^{\Delta LPC}$-mice did not develop HCC. The important function of NEMO in our model, however, became obvious in the context of MYC-induced primary liver cancer.

Constitutive activation of NF-κB was suggested to contribute to hepatocarcinogenesis by accelerating the neoplastic development of MYC-transformed cells [29]. Our results indicate a distinct function of NF-κB in MYC-induced liver cancer. NEMO deletion increased hepatocyte apoptosis and regenerative proliferation, both in the presence and absence of MYC overexpression. Importantly, NEMO deletion led to an increase in infiltrating inflammatory cells. These findings are consistent with the results of Luedde et al., who described increased apoptotic death of hepatocytes, increased regeneration and increased immune cell infiltration into the liver parenchyma in 8-week old mice with liver-specific deletion of NEMO [9]. In general, increased apoptosis is not uncommon in liver tumors; it may even correlate with increased proliferation. Still, it is not yet entirely clear what is cause and what is effect, e.g. whether apoptosis is a side effect of increased stress due to increased proliferation, or whether apoptosis vice versa may create conditions that promote a compensatory response with hyperproliferation and eventually tumorigenesis [30].

Importantly, NEMO deletion modified the phenotype of primary liver tumors since we observed an additional tumor component resembling intrahepatic cholangiocarcinoma (ICC). ICC has not been reported in mouse models of MYC-induced HCC previously. Tumor nodules found in $MYC^{LAP\text{-}tTA}/NEMO^{\Delta LPC}$ livers resemble the classic type of combined hepatocellular cholangiocarcinoma (cHCC-CC), which is a rare and aggressive form of primary liver cancer with features of both hepatocytic and biliary differentiation [31]. The modulation of the tumor phenotype towards cholangiocarcinoma was accompanied by MAPK activation, reflecting previous data on the importance of that pathway in cholangiocarcinoma [32].

According to the latest WHO classification in 2010 [31], cHCC-CC can be divided into two subtypes: classical type and cHCC-CC with stem cell features. The latter is further subcategorized into three subtypes: typical subtype, intermediate cell subtype and cholangiolocellular subtype. Clinical studies have shown that cHCC-CC appears to exhibit a more aggressive biological behavior and poorer prognosis than HCC [33,34]. However, the cell of origin of cHCC-CC has not been well defined [16]. Two possibilities have been suggested, differentiation of HCC or CC into the other component or derivation from hepatic progenitor cells [35,36].

Luedde et al. in their study on mice with liver-specific deletion of NEMO observed a strong activation of hepatic progenitor and oval cells [9], and we wondered whether we could observe a similar phenomenon and whether we could characterize the cell type giving rise to the ICC-like tumor component in $MYC^{LAP\text{-}tTA}/NEMO^{\Delta LPC}$ mice. Indeed, in ICC-like areas, we could observe abundant cells expressing the biliary/progenitor markers Sox9 and CK19, while expression of the mature hepatocyte marker CPS1 was mostly absent. Furthermore, gene expression analysis of hepatocytic progenitor markers showed a significant upregulation of mRNA levels of CK19, CK7, and Epcam in $MYC^{LAP\text{-}tTA}/NEMO^{\Delta LPC}$ mice.

Sox9-positive ductal progenitor cells can give rise to oval cell proliferation, but rarely produce hepatocytes in vivo [37]. Therefore, it is reasonable to hypothesize that these Sox9-positive progenitor cells may contribute to the development of the ICC component of cHCC-CC. Of note, HCC can also express the progenitor cell/ductular marker CK19, and CK19 expression in HCC is associated with a more aggressive clinical course and poorer prognosis [38,39].

Characteristic for the ICC component of cHCC-CC is the desmoplastic reaction. We verified this by Sirius red staining and immunofluorescence staining of αSMA, which showed a strong activation of hepatic stellate cells surrounding the ICC-like structure. We therefore speculate that cHCC-CC found in $MYC^{LAP\text{-}tTA}/NEMO^{\Delta LPC}$ mice may originate from hepatic progenitor cells.

Previous studies have shown that the Raf-MEK-MAPK signaling pathway may play an important role in the development of HCC. Our data indeed showed activation of Erk and JNK in $MYC^{LAP\text{-}tTA}$ and $MYC^{LAP\text{-}tTA}/NEMO^{\Delta LPC}$ mice, being more pronounced in the latter group. Also, we found that NEMO ablation led to an upregulation of pSTAT3 levels. As behavior and phenotype of HCC can be influenced by the inflammatory milieu that depends on the driving oncogenes [40]. It is plausible that the chronic inflammatory milieu caused by NEMO ablation modulates the phenotype and aggressiveness of our liver tumors.

In summary, found that liver specific NEMO ablation accelerates MYC-induced tumorigenesis, at least in part due to the more aggressive and heterogenous tumor nodules generated, i.e. cHCC-CC. Due to lack of an animal model for cHCC-CC, the role of hepatic progenitor cells as the cell of origin has been rarely investigated. Our mouse model of $MYC^{LAP\text{-}tTA}/NEMO^{\Delta LPC}$ offers the potential to investigate the cell of origin and molecular mechanisms driving cHCC-CC. Our data also suggest that NEMO in hepatocytes exerts a protective role during MYC-induced HCC, by limiting apoptosis and inflammatory infiltration. In view of our findings, targeting the IKK/NF-κB pathway as option for HCC therapy should be considered with caution since it might accelerate tumor growth.

Author contributions

JH, MG, LKC and HJM carried out experiments and analyzed data. FL and MMY analyzed data. HJM and TW designed the study, conceived experiments and analyzed data. JH, HJM and TW wrote the paper. All authors had final approval of the submitted and published versions.

Conflicts of interest

The authors declare no conflict of interest. H. J. M. is an employee of Novartis Oncology, which was not involved in the study.

Acknowledgments

We thank Uta Manfras for excellent technical assistance.

Appendix A. Supplementary data

Supplementary data to this article can be found online at https://doi.org/10.1016/j.canlet.2019.05.023.

References

[1] J.M. Llovet, J. Zucman-Rossi, E. Pikarsky, B. Sangro, M. Schwartz, M. Sherman, G. Gores, Hepatocellular carcinoma, Nature reviews. Disease primers 2 (2016)

16018.
[2] F.R. Greten, L. Eckmann, T.F. Greten, J.M. Park, Z.W. Li, L.J. Egan, M.F. Kagnoff, M. Karin, IKKbeta links inflammation and tumorigenesis in a mouse model of colitis-associated cancer, Cell 118 (2004) 285–296.
[3] Q. Li, D. Van Antwerp, F. Mercurio, K.F. Lee, I.M. Verma, Severe liver degeneration in mice lacking the IkappaB kinase 2 gene, Science 284 (1999) 321–325.
[4] M. Grossmann, D. Metcalf, J. Merryfull, A. Beg, D. Baltimore, S. Gerondakis, The combined absence of the transcription factors Rel and RelA leads to multiple hemopoietic cell defects, Proc. Natl. Acad. Sci. U. S. A. 96 (1999) 11848–11853.
[5] G.W. Vainer, E. Pikarsky, Y. Ben-Neriah, Contradictory functions of NF-kappaB in liver physiology and cancer, Cancer Lett. 267 (2008) 182–188.
[6] M. Arsura, L.G. Cavin, Nuclear factor-kappaB and liver carcinogenesis, Cancer Lett. 229 (2005) 157–169.
[7] E. Pikarsky, R.M. Porat, I. Stein, R. Abramovitch, S. Amit, S. Kasem, E. Gutkovich-Pyest, S. Urieli-Shoval, E. Galun, Y. Ben-Neriah, NF-kappaB functions as a tumour promoter in inflammation-associated cancer, Nature 431 (2004) 461–466.
[8] Y. Sunami, M. Ringelhan, E. Kokai, M. Lu, T. O'Connor, A. Lorentzen, A. Weber, A.K. Rodewald, B. Mullhaupt, L. Terracciano, S. Gul, S. Wissel, F. Leithauser, D. Krappmann, P. Riedl, D. Hartmann, R. Schirmbeck, P. Strnad, N. Huser, J. Kleeff, H. Friess, R.M. Schmid, F. Geisler, T. Wirth, M. Heikenwalder, Canonical NF-kappaB signaling in hepatocytes acts as a tumor-suppressor in hepatitis B virus surface antigen-driven hepatocellular carcinoma by controlling the unfolded protein response, Hepatology 63 (2016) 1592–1607.
[9] T. Luedde, N. Beraza, V. Kotsikoris, G. van Loo, A. Nenci, R. De Vos, T. Roskams, C. Trautwein, M. Pasparakis, Deletion of NEMO/IKKgamma in liver parenchymal cells causes steatohepatitis and hepatocellular carcinoma, Cancer Cell 11 (2007) 119–132.
[10] T. Sakurai, S. Maeda, L. Chang, M. Karin, Loss of hepatic NF-kappa B activity enhances chemical hepatocarcinogenesis through sustained c-Jun N-terminal kinase 1 activation, Proc. Natl. Acad. Sci. U. S. A. 103 (2006) 10544–10551.
[11] V. Kondylis, A. Polykratis, H. Ehlken, L. Ochoa-Callejero, B.K. Straub, S. Krishna-Subramanian, T.M. Van, H.M. Curth, N. Heise, F. Weih, U. Klein, P. Schirmacher, M. Kelliher, M. Pasparakis, NEMO prevents steatohepatitis and hepatocellular carcinoma by inhibiting RIPK1 kinase activity-mediated hepatocyte apoptosis, Cancer Cell 28 (2015) 830.
[12] C.M. Shachaf, A.M. Kopelman, C. Arvanitis, A. Karlsson, S. Beer, S. Mandl, M.H. Bachmann, A.D. Borowsky, B. Ruebner, R.D. Cardiff, Q. Yang, J.M. Bishop, C.H. Contag, D.W. Felsher, MYC inactivation uncovers pluripotent differentiation and tumour dormancy in hepatocellular cancer, Nature 431 (2004) 1112–1117.
[13] E. Santoni-Rugiu, M.R. Jensen, V.M. Factor, S.S. Thorgeirsson, Acceleration of c-myc-induced hepatocarcinogenesis by Co-expression of transforming growth factor (TGF)-alpha in transgenic mice is associated with TGF-beta1 signaling disruption, Am. J. Pathol. 154 (1999) 1693–1700.
[14] C.E. Nesbit, J.M. Tersak, E.V. Prochownik, MYC oncogenes and human neoplastic disease, Oncogene 18 (1999) 3004–3016.
[15] S. Beer, A. Zetterberg, R.A. Ihrie, R.A. McTaggart, Q. Yang, N. Bradon, C. Arvanitis, L.D. Attardi, S. Feng, B. Ruebner, R.D. Cardiff, D.W. Felsher, Developmental context determines latency of MYC-induced tumorigenesis, PLoS Biol. 2 (2004) e332.
[16] E. Brunt, S. Aishima, P.A. Clavien, K. Fowler, Z. Goodman, G. Gores, A. Gouw, A. Kagen, D. Klimstra, M. Komuta, F. Kondo, R. Miksad, M. Nakano, Y. Nakanuma, I. Ng, V. Paradis, Y. Nyun Park, A. Quaglia, M. Roncalli, T. Roskams, M. Sakamoto, R. Saxena, C. Sempoux, C. Sirlin, A. Stueck, S. Thung, W.M.S. Tsui, X.W. Wang, A. Wee, H. Yano, M. Yeh, Y. Zen, J. Zucman-Rossi, N. Theise, cHCC-CCA, Consensus terminology for primary liver carcinomas with both hepatocytic and cholangiocytic differentation, Hepatology 68 (2018) 113–126.
[17] A. Kistner, M. Gossen, F. Zimmermann, J. Jerecic, C. Ullmer, H. Lubbert, H. Bujard, Doxycycline-mediated quantitative and tissue-specific control of gene expression in transgenic mice, Proc. Natl. Acad. Sci. U. S. A. 93 (1996) 10933–10938.
[18] D. Marinkovic, T. Marinkovic, B. Mahr, J. Hess, T. Wirth, Reversible lymphomagenesis in conditionally c-MYC expressing mice, Int. J. Cancer 110 (2004) 336–342.
[19] C. Postic, M.A. Magnuson, DNA excision in liver by an albumin-Cre transgene occurs progressively with age, Genesis 26 (2000) 149–150.
[20] M. Schmidt-Supprian, W. Bloch, G. Courtois, K. Addicks, A. Israel, K. Rajewsky, M. Pasparakis, NEMO/IKK gamma-deficient mice model incontinentia pigmenti, Mol. Cell 5 (2000) 981–992.
[21] T.R. Kress, P. Pellanda, L. Pellegrinet, V. Bianchi, P. Nicoli, M. Doni, C. Recordati, S. Bianchi, L. Rotta, T. Capra, M. Rava, A. Verrecchia, E. Radaelli, T.D. Littlewood, G.I. Evan, B. Amati, Identification of MYC-dependent transcriptional programs in oncogene-addicted liver tumors, Cancer Res. 76 (2016) 3463–3472.
[22] S. Vijgen, B. Terris, L. Rubbia-Brandt, Pathology of intrahepatic cholangiocarcinoma, Hepatobiliary Surg. Nutr. 6 (2017) 22–34.
[23] L. Li, G.D. Zhao, Z. Shi, L.L. Qi, L.Y. Zhou, Z.X. Fu, The Ras/Raf/MEK/ERK signaling pathway and its role in the occurrence and development of HCC, Oncol Lett 12 (2016) 3045–3050.
[24] S. Wan, E. Zhao, I. Kryczek, L. Vatan, A. Sadovskaya, G. Ludema, D.M. Simeone, W. Zou, T.H. Welling, Tumor-associated macrophages produce interleukin 6 and signal via STAT3 to promote expansion of human hepatocellular carcinoma stem cells, Gastroenterology 147 (2014) 1393–1404.
[25] J. Ji, T. Eggert, A. Budhu, M. Forgues, A. Takai, H. Dang, Q. Ye, J.S. Lee, J.H. Kim, T.F. Greten, X.W. Wang, Hepatic stellate cell and monocyte interaction contributes to poor prognosis in hepatocellular carcinoma, Hepatology 62 (2015) 481–495.
[26] H. Okabe, T. Beppu, H. Hayashi, T. Ishiko, T. Masuda, R. Otao, H. Horlad, H. Jono, M. Ueda, S. Shinriki, Y. Ando, H. Baba, Hepatic stellate cells accelerate the malignant behavior of cholangiocarcinoma cells, Ann. Surg. Oncol. 18 (2011) 1175–1184.
[27] T. Amann, F. Bataille, T. Spruss, M. Muhlbauer, E. Gabele, J. Scholmerich, P. Kiefer, A.K. Bosserhoff, C. Hellerbrand, Activated hepatic stellate cells promote tumorigenicity of hepatocellular carcinoma, Cancer Sci. 100 (2009) 646–653.
[28] C. Kordes, I. Sawitza, S. Gotze, D. Herebian, D. Haussinger, Hepatic stellate cells contribute to progenitor cells and liver regeneration, J. Clin. Investig. 124 (2014) 5503–5515.
[29] V. Factor, A.L. Oliver, G.R. Panta, S.S. Thorgeirsson, G.E. Sonenshein, M. Arsura, Roles of Akt/PKB and IKK complex in constitutive induction of NF-kappaB in hepatocellular carcinomas of transforming growth factor alpha/c-myc transgenic mice, Hepatology 34 (2001) 32–41.
[30] Y. Boege, M. Malehmir, M.E. Healy, K. Bettermann, A. Lorentzen, M. Vucur, A.K. Ahuja, F. Bohm, J.C. Mertens, Y. Shimizu, L. Frick, C. Remouchamps, K. Mutreja, T. Kahne, D. Sundaravinayagam, M.J. Wolf, H. Rehrauer, C. Koppe, T. Speicher, S. Padrissa-Altes, R. Maire, J.M. Schattenberg, J.S. Jeong, L. Liu, S. Zwirner, R. Boger, N. Huser, R.J. Davis, B. Mullhaupt, H. Moch, H. Schulze-Bergkamen, P.A. Clavien, S. Werner, L. Borsig, S.A. Luther, P.J. Jost, R. Weinlich, K. Unger, A. Behrens, L. Hillert, C. Dillon, M. Di Virgilio, D. Wallach, E. Dejardin, L. Zender, M. Naumann, H. Walczak, D.R. Green, M. Lopes, I. Lavrik, T. Luedde, M. Heikenwalder, A. Weber, A dual role of caspase-8 in triggering and sensing proliferation-associated DNA damage, a key determinant of liver cancer development, Cancer Cell 32 (2017) 342–359 e310.
[31] J.F. Flejou, [WHO Classification of digestive tumors: the fourth edition], Ann. Pathol. 31 (2011) S27–S31.
[32] C. Wang, T. Maass, M. Krupp, F. Thieringer, S. Strand, M.A. Worns, A.P. Barreiros, P.R. Galle, A. Teufel, A systems biology perspective on cholangiocellular carcinoma development: focus on MAPK-signaling and the extracellular environment, J. Hepatol. 50 (2009) 1122–1131.
[33] X. Yin, B.H. Zhang, S.J. Qiu, Z.G. Ren, J. Zhou, X.H. Chen, Y. Zhou, J. Fan, Combined hepatocellular carcinoma and cholangiocarcinoma: clinical features, treatment modalities, and prognosis, Ann. Surg. Oncol. 19 (2012) 2869–2876.
[34] G. Sapisochin, N. Fidelman, J.P. Roberts, F.Y. Yao, Mixed hepatocellular cholangiocarcinoma and intrahepatic cholangiocarcinoma in patients undergoing transplantation for hepatocellular carcinoma, Liver Transplant. 17 (2011) 934–942.
[35] M.M. Yeh, Pathology of combined hepatocellular-cholangiocarcinoma, J. Gastroenterol. Hepatol. 25 (2010) 1485–1492.
[36] F. Zhang, X.P. Chen, W. Zhang, H.H. Dong, S. Xiang, W.G. Zhang, B.X. Zhang, Combined hepatocellular cholangiocarcinoma originating from hepatic progenitor cells: immunohistochemical and double-fluorescence immunostaining evidence, Histopathology 52 (2008) 224–232.
[37] B.D. Tarlow, M.J. Finegold, M. Grompe, Clonal tracing of Sox9+ liver progenitors in mouse oval cell injury, Hepatology 60 (2014) 278–289.
[38] M. Takano, K. Shimada, T. Fujii, K. Morita, M. Takeda, Y. Nakajima, A. Nonomura, N. Konishi, C. Obayashi, Keratin 19 as a key molecule in progression of human hepatocellular carcinomas through invasion and angiogenesis, BMC Canc. 16 (2016) 903.
[39] O. Govaere, M. Komuta, J. Berkers, B. Spee, C. Janssen, F. de Luca, A. Katoonizadeh, J. Wouters, L.C. van Kempen, A. Durnez, C. Verslype, J. De Kock, V. Rogiers, L.A. van Grunsven, B. Topal, J. Pirenne, H. Vankelecom, F. Nevens, J. van den Oord, M. Pinzani, T. Roskams, Keratin 19: a key role player in the invasion of human hepatocellular carcinomas, Gut 63 (2014) 674–685.
[40] M.S. Matter, J.U. Marquardt, J.B. Andersen, C. Quintavalle, N. Korokhov, J.K. Stauffer, K. Kaji, T. Decaens, L. Quagliata, F. Elloumi, T. Hoang, A. Molinolo, E.A. Conner, A. Weber, M. Heikenwalder, V.M. Factor, S.S. Thorgeirsson, Oncogenic driver genes and the inflammatory microenvironment dictate liver tumor phenotype, Hepatology 63 (2016) 1888–1899.